Atmos. Chem. Phys. Discuss., 14, 23555–23581, 2014
www.atmos-chem-phys-discuss.net/14/23555/2014/
doi:10.5194/acpd-14-23555-2014

Atmospheric Chemistry and Physics Discussions

Competition between core and periphery-based processes in warm convective clouds – from invigoration to suppression

G. Dagan, I. Koren, and O. Altaratz

Department of Earth and Planetary Sciences, The Weizmann Institute, Rehovot 76100, Israel

Received: 17 August 2014 – Accepted: 29 August 2014 – Published: 12 September 2014

Correspondence to: I. Koren (ilan.koren@weizmann.ac.il)

Published by Copernicus Publications on behalf of the European Geosciences Union.

Abstract

How do changes in the amount and properties of aerosol affect warm clouds? Recent studies suggest that they have opposing effects. Some suggest that an increase in aerosol loading leads to enhanced evaporation and therefore smaller clouds, whereas other studies suggest clouds' invigoration. In this study, using a bin-microphysics cloud model, we propose a theoretical scheme that analyzes the evolution of key processes in warm clouds, under different aerosol loading and environmental conditions, to explain this contradiction.

Such a framework reveals a robust reversal in the trend of the clouds' response to an increase in aerosol loading. When aerosol conditions are shifted from super-pristine to slightly pollute, the clouds formed are deeper and have a larger water mass. Such a trend continues up to an optimal concentration (N_{op}) that allows the cloud to achieve a maximal water mass. Hence, for any concentration below N_{op} the cloud formed contains less mass and therefore can be considered as aerosol limited, whereas for concentrations greater than N_{op} cloud periphery processes, such as enhanced entrainment, take over leading to cloud suppression. We show that N_{op} is a function of the thermodynamic conditions (temperature and humidity profiles). Thus, profiles that favor deeper clouds would dictate larger values of N_{op}, whereas for profiles of shallow convective clouds, N_{op} corresponds to the pristine range of the aerosol loading.

Such a view of a trend reversal, marked by the optimal concentration, N_{op}, helps one to bridge the gap between the contradictory results of numerical models and observations. Satellite studies are biased in favor of larger clouds that are characterized by larger N_{op} values and therefore invigoration is observed. On the other hand, modeling studies are biased in favor of small, mostly trade-like convective clouds, which are characterized by low N_{op} values (in the pristine range), and therefore cloud suppression is mostly reported as a response to an increase in aerosol loading.

ACPD
14, 23555–23581, 2014

1 Introduction

Clouds play an important role in the Earth's energy balance (Baker and Peter, 2008) and the hydrological cycle. The clouds' macrophysical properties, such as coverage and the vertical extent as well as microphysical properties like liquid water content (LWC), particle size, shape, and phase determine the cloud's interaction with electromagnetic radiation. Because of the inherent variance in cloud types and properties and the complexity of the processes, clouds are responsible for the greatest uncertainty in climate research (Forster et al., 2007; Boucher et al., 2013). To better understand the role of clouds in the current climate system and to be able to predict their properties under different climate change scenarios, we must advance our understanding of those processes and environmental factors that affect cloud properties.

Aerosols act as cloud condensation nuclei (CCN), on which droplets can form, and as ice nuclei (IN), for the initial creation of ice particles. A theoretically clean atmosphere with no aerosols is suggested to be mostly cloud free (Reutter et al., 2009; Koren et al., 2014). CCN enable the nucleation of droplets by reducing the supersaturation required for the process. Without CCN, droplets would form at supersaturation levels of several hundred percent by homogenous nucleation. However, in the presence of CCN, droplets are formed by a heterogeneous nucleation process, which requires an order of one percent supersaturation (Wilson, 1897; Pruppacher and Klett, 1978). The availability, size distribution, and chemical properties of aerosols govern the initial number and size distribution of the droplets. Polluted clouds initially have smaller and more numerous droplets, with smaller variance (Squires, 1958; Squires and Twomey, 1960; Warner and Twomey, 1967; Fitzgerald and Spyers-Duran, 1973; Twomey, 1977).

The change in the initial droplet size distribution affects key processes and the interactions between them. For a given total liquid water mass (or volume), the total surface area of smaller droplets is larger and therefore, the condensation process is more efficient under the given supersaturation conditions. On the other hand, similarly, under subsaturation conditions, smaller droplets evaporate more efficiently and

ACPD
14, 23555–23581, 2014

may enhance the mixing processes due to the evaporative cooling-induced downdrafts (Xue and Feingold, 2006; Jiang et al., 2006; Small et al., 2009). These two processes create an interesting competition controlled by the relative humidity (RH) conditions in different regions of the clouds and in its surroundings.

The collision-coalescence and rain processes are impacted by the change in the droplets' size distribution as well. There is a delay in the initiation of the collision-coalescence process in polluted clouds (Gunn and Phillips, 1957; Squires, 1958; Warner, 1968; Albrecht, 1989). These microphysical processes were suggested to be coupled to dynamical ones and in the case of convective clouds to form the baseline for the invigoration effect (Andreae et al., 2004; Koren et al., 2005; Rosenfeld et al., 2008; Tao et al., 2012; Fan et al., 2013; Altaratz et al., 2014). Surface rain, as the end result of all the cloud's feedbacks, was shown to be affected by changes in aerosol loading as well (Levin and Cotton, 2009; Khain, 2009; Koren et al., 2012).

For warm convective clouds (containing only liquid water drops) the overall effect of the addition of aerosols on the clouds' macrophysical properties is still considered an open question and studies show contradictory results. There are few observational studies that show cloud invigoration by aerosols. Kaufman et al. (2005) found an increase in cloud coverage under polluted, smoky, and dusty conditions over the transition zone between stratocumulus to cumulus clouds over the tropical Atlantic Ocean. Yuan et al. (2011) showed a larger coverage of trade cumulus clouds and higher clouds top associated with volcanic aerosols near Hawaii. Koren et al. (2014) have recently shown that convective clouds over the Southern Oceans are "aerosol limited" up to moderate aerosol loading conditions. They showed that as the AOD increases, warm convective clouds exhibit invigoration, manifested as deeper clouds with larger areas.

On the other hand, some observational studies like that of Li et al. (2011), who studied warm clouds over the southern great plains of the United States, reported that aerosol did not affect the clouds' top height.

Numerical studies of an aerosol's effect on warm cumulus clouds show either no effect, or in contrast with invigoration, they show suppression. Jiang and Feingold (2006)

ACPD
14, 23555–23581, 2014

found that an increase in aerosol loading in fields of warm shallow convective clouds results in reduced precipitation. However, the clouds do not undergo significant changes in LWP, cloud fraction, and cloud depth. Xue et al. (2008) found that the addition of aerosols leads to smaller clouds and suppression of precipitation.

Here we used a single cloud model to study how changes in aerosol loading affect warm convective clouds at the process level, with a dependency on the environmental conditions. More specifically, we describe the evolution in time and the competition between key processes. Whereas a single cloud model might be quite simplistic in capturing the dynamic processes on the whole cloud scale and does not account for larger (cloud field) scales. However, the essential microphysical and dynamical processes affecting finer scales are well captured and are the focus of this study.

2 Methodology

We used the Tel Aviv University axisymmetric nonhydrostatic cloud model (TAU-CM) with a detailed treatment of cloud microphysics (Tzivion et al., 1994; Reisin et al., 1996). The warm microphysical processes included are nucleation of CCN, condensation and evaporation, collision-coalescence, binary breakup, and sedimentation. The microphysical processes are formulated and solved using a multi-moment bin method (Tzivion et al., 1987).

To better understand the role of key environmental factors, we ran the model with 9 different initial conditions based on theoretical atmospheric profiles that characterize a moist tropical environment. Each of the profiles includes a well-mixed subcloud layer between 0 and ~ 1000 m, a conditionally unstable cloud layer between 1000 and 6000 m (T1), 4000 m (T2), and 2000 m (T3), and an overlying inversion layer. We assigned 3 dew-point temperature profiles (T_d) equivalent to 95 % relative humidity in the cloudy layer (RH1), 90 % (RH2), and 80 % (RH3) to each of the Temperature (T1, T2, or T3) profiles (all together 9 profiles). The profiles are denoted here by a combination of the letters describing the temperature and humidity, like T1RH1 or T1RH2 and so on.

ACPD
14, 23555–23581, 2014

The relative humidity above the inversion layer is 30 % in all the profiles. The inversion layer has a temperature gradient of 2 °C over 50 m. Figure 1 presents 3 of the initial profiles: T1 combined with RH1 (T1RH1), T2 with RH2 (T2RH2), and T3 with RH3 (T3RH3). In the deeper clouds cases the cloud's top temperature is around −10 °C; thus, there is a small likelihood that we neglect the formation of small amounts of ice. For each initial atmospheric profile we ran the model with 10 different levels of aerosol concentrations, in the range of 5–10 000 cm^{-3} (all together 90 simulations). The background aerosol size distribution represents a maritime clean environment (Jaenicke, 1988). The aerosols are assumed to be composed of NaCl. In the clean cases (5, 25, 125, and 250 cm^{-3}) the basic marine size distribution (~ 290 cm^{-3}) was divided by a constant factor in order to obtain the requested concentration (while the shape of the size distribution was kept constant). In the polluted cases (500, 1000, 2000, 3000, 4000, and 10 000 cm^{-3}) we added to the background size distribution a log-normal distribution in sizes ranging between 0.012–0.844 µm in order to represent anthropogenic pollution. In this study, to reduce the complexity, we avoided the effect of giant CCN (GCCN) (Feingold et al., 1999; Yin et al., 2000) by truncating the aerosol size distribution at 1 µm. The model resolution was set to 50 m both in the vertical and horizontal directions, with a time step of 1 s. The convection was initiated by a warm bubble of 3 °C at one grid point near the bottom of the domain.

Analysis of the effect of aerosol on convective clouds under different environmental conditions and understanding the role of key cloud processes require simulation of many different clouds. Moreover, as we follow the time evolution of each process for each case, the size of the output dataset of the runs becomes large. To reduce the dimensionally of the results of our 90 simulations and to distill the essence of the interplay between processes, we focused on the magnitude and timing of key processes in the cloud's evolution.

ACPD
14, 23555–23581, 2014

3 Results and discussion

First we examined the bulk properties of clouds (on a whole cloud scale) of all the simulated clouds as a function of the aerosol loading.

Figure 2 presents the maximum cloud total mass for each cloud simulation as a function of the aerosol concentration used for the same simulation. Each curve represents the results of 10 different simulations performed for each of the 9 different initialization profiles (3 profiles of temperature combined with 3 different levels of RH in the cloudy layer). For all the profile curves the maximum total cloud mass increases with the increase in aerosol loading until a maximum point is reached, where above it, the simulated clouds have smaller maximal masses. We defined here the optimal aerosol concentration (N_{op}) as the concentration that is associated with the simulated cloud with the largest maximum total liquid water mass per profile. In most cases, the N_{op} value is larger for profiles characterized by a higher inversion base height and a higher RH value in the cloudy layer (a more humid environment).

The clouds' maximal total water mass, as presented in Fig. 2, represents the result of interactions of various clouds' internal processes that determine the clouds' properties at any given time. To understand the impact of aerosol on these processes and on the interactions between them, we followed the timing and magnitude of key microphysical processes in different clouds that were formed under the same environmental conditions (the same initialization profile), but with a different aerosol loading. Figures 3 and 4 present the results of 3 clouds that were formed under the conditions of profile T1RH1 with aerosol loading levels of 125, 1000, and 4000 cm^{-3} (denoted hereafter as T1RH1_125, T1RH1_1000, and T1RH1_4000). The results presented in Fig. 3 include the time evolution of three major cloud processes: diffusion (condensation/evaporation), collision-coalescence, and surface rain. The three curves represent: (1) the total net condensed and evaporated mass in the cloud per unit time (the water vapor mass that was transferred to liquid, blue curves), (2) the total collected mass in the cloud per unit time (the mass transferred from small to bigger size bins, red

ACPD
14, 23555–23581, 2014

curves), and (3) the surface rain mass per unit time (green curves). Figure 4 presents the time evolution of the total water mass and the total droplet surface area for those three clouds.

The differences in the magnitude and timing of the process, among the three clouds, presented in Fig. 3, reveal an interesting interplay between processes. The total condensed mass along the whole lifetime of the cloud (summed over all grid points with supersaturation) is 1.9×10^8 kg in the clean cloud case (T1RH1_125), whereas it is 4.7×10^8 kg for the polluted cloud (T1RH1_4000). Difference in the total condensed mass are due to increased efficiency of the condensation process and the delay in the collision-coalescence process, in the polluted cloud.

The condensation efficiency is determined by the droplets' surface area (Fig. 4). The total droplet surface area of cloud T1RH1_4000 at the time of its maximum total mass (1.2×10^7 kg) is 4.4×10^9 m^2, which yields a surface-area-to-mass ratio of 366.7 m^2 kg^{-1}. For the clean cloud, T1RH1_125, the maximum total mass is 7.1×10^6 kg, with a droplet surface area of 1.9×10^8 m^2, which yields a surface-area-to-mass ratio of 26.8 m^2 kg^{-1}. Therefore, the polluted cloud has a much higher droplet surface area per unit of water mass. It is maintained throughout the clouds' lifetime, with a mean surface-area-to-mass ratio of 79.0 and 312.8 m^2 kg^{-1} for the clean and polluted clouds, respectively.

Moreover, the polluted cloud has a longer time for efficient condensational growth due to the delay in the initiation of the collision-coalescence. Whereas for the clean cloud case (T1RH1_125) the peaks of the collision-coalescence and condensation processes are relatively close in time (at 56 and 59 min of simulation, respectively), with the one of the collision-coalescence processes slightly ahead, in the more polluted clouds the peak in the collision-coalescence process is delayed and appears after the peak in condensation (1 min delay for the 1000 cm^{-3} case and 14 min for the 4000 cm^{-3} case). In the clean cloud case (T1RH1_125) the small number of droplets grows rapidly with almost no competition on the available water vapor. To demonstrate this point, we examined the early stages of the clouds' development. Five minutes after the clouds had formed, at the point of maximum liquid water content, cloud T1RH1_125

ACPD
14, 23555–23581, 2014

(T1RH1_4000) had a mean droplet radius of 7.4 µm (2.3 µm) with a standard deviation of 2.5 µm (0.4 µm).

The mean radius is larger and the size distribution is wider for the clean case so the droplets reach the critical size for collisions rapidly and the collision-coalescence process starts almost immediately after the condensation start. The early initiation of the collision-coalescence process acts as positive feedback for this aerosol effect on the condensed mass and further reduces the droplets' surface area (Fig. 4). The less effective integrated condensation prevents the clean clouds from consuming more of the available supersaturation. The condensation peaks at 56 min of simulation for the T1RH1_125 clean cloud (with 2.4 % of mean supersaturation in the supersaturated region in the cloud), compared with 78 min (with 0.05 % of mean supersaturation) in the T1RH1_4000 case. On the same note, the early initiation of the collision-coalescence process in the clean cloud also drives an early start of the rainout from the cloud. The early rainout leads to mass transfer downward and therefore an increased drag force at the lower part of the cloud that further impedes the cloud's development. The clean cloud consumes a small amount of water vapor (a smaller total mass, as can be seen in Fig. 4), and rainout early (Fig. 3). On the other hand, the delay in the onset of the collision-coalescence process in the most polluted cloud (T1RH1_4000, see Fig. 3 lower panel) allows the entrainment to act for a longer time (after the peak in condensation) and thus, enhances the evaporation; this consequently, reduces the cloud's liquid water mass. The total evaporated mass along the entire lifetime of the cloud (integrated over all cloud grid points with subsaturation), in the clean cloud case (T1RH1_125) is 1.7×10^8 kg, whereas it is 3.5×10^8 kg for the polluted cloud (T1RH1_4000). This results in delayed and weaker precipitation from the polluted clouds (in Fig. 3 we present the results of the most humid profile, so this effect is less significant than in the other profiles). Such competition between opposing processes yields an optimal aerosol concentration for the total cloud mass as well as for the rain yield, with a value in between the two examples. Figures 2 and 3 show that for the total cloud mass and peak rain

ACPD
14, 23555–23581, 2014

(the maximal rain rate), a concentration of around 1000 cm^{-3} results in larger values compared with 125 cm^{-3} and 4000 cm^{-3}.

When the impact of aerosol on the time difference between the onset and peaks of key processes is explored further, one can see that for the more polluted clouds the time lag between the peaks in the condensation mass and the collision-coalescence mass per unit time is longer (Fig. 5). Note that in the extreme polluted cases, for some of the initialization profiles the collision-coalescence process is almost totally suppressed, and therefore their information is not presented in the figure. In the cleaner cases, driven by efficient collection, the maximum collected mass per unit time appears before the maximum in the condensed mass (see the negative values of the time difference in Fig. 5) even though the condensation process obviously starts earlier.

We note that the delay in the onset of the collision-coalescence process in the polluted clouds has two opposing effects on the updraft. The first one, as was mentioned before, delays the reduction in the integrated droplets' surface area and maintains an effective condensation process (that is originally more effective in the polluted clouds). The more efficient condensation leads to a stronger latent heat release that supports the positive buoyancy of the cloud. On the other hand, a delay in the collision-coalescence implies a delay in the droplet sedimentation and therefore, later as the droplets' mass accumulates, the updraft is reduced due to increased drag force.

As for periphery processes, since stronger downdrafts, driven by the evaporation, induce stronger horizontal winds (Altaratz et al., 2008), the magnitude of the horizontal winds near the cloud margins can serve as a measure of the entrainment strength. In agreement with previous studies: (Xue and Feingold, 2006; Jiang et al., 2006; Small et al., 2009), the polluted clouds exhibit stronger horizontal wind velocity for all profiles. For example, for the T1RH1 profiles the mean horizontal winds averaged along the cloud margins were 0.18 $m\,s^{-1}$, 0.24 $m\,s^{-1}$, and 0.34 $m\,s^{-1}$ for T1RH1_125, T1RH1_1000, and T1RH1_4000, respectively.

ACPD
14, 23555–23581, 2014

We see that similarly to the condensation argument, the ratio of drops surface-area-to-volume increases with increasing aerosol concentration (see Fig. 4), meaning that the smaller droplets evaporate more efficiently (Xue and Feingold, 2006).

The evaporation is enhanced by positive feedback because the enhanced downdrafts at the cloud's periphery further increase the mixing of outer air into the cloud. The magnitude of this effect strongly depends on the environmental humidity. As the humidity increases, the relative effect of the entrainment process decreases.

Similarly to the droplets' scale, the size of the whole cloud plays an important role in controlling the entrainment impact. Larger clouds have a smaller surface area (A) to volume (V) ratio ($\eta = AV^{-1}$) and therefore, a smaller portion of them comes in direct contact with the drier surroundings (Simpson, 1971; Stirling and Stratton, 2012). For example, at the maximal mass stage η (T1RH1_500) = 0.0062 m^{-1}, whereas η (T3RH3_500) = 0.011 m^{-1}, which is almost double. The larger the value of η, the stronger periphery-based (suppression) processes can be expected.

The competing effects discussed above show that, on the one hand, more aerosols result in enhanced condensation (higher efficiency and for a longer time), and with a stronger latent heat release, which leads to deeper clouds with a larger water mass. On the other hand, more aerosols induce mass accumulation that enhances drag forces and stronger entrainment-driven evaporation, which eventually leads to mass reduction and smaller clouds. The contest, between the invigoration to the suppression processes, poses the existence of an optimal value (N_{op}) with respect to the cloud mass, which dictates a change in the sign of the trend regarding the cloud mass response to an increase in aerosol loading (Fig. 2). At low values of aerosol loading, as long as the cloud can still consume the supersaturation, the addition of aerosols leads to cloud invigoration. As the concentration approaches N_{op}, the enhanced entrainment-driven evaporation, as well as the contribution of the drag-force, builds up a counter effect to the enhancement. Above the N_{op} value, the suppression processes take over. The value of N_{op} strongly depends on the environmental conditions. As the inversion's base height increases (increasing the potential cloud depth and therefore reducing

ACPD
14, 23555–23581, 2014

the cloud's surface-area-to-volume ratio) and/or the RH of the cloudy layer increases, the entrainment impact weakens and therefore, N_{op} increases. For similar temperature profiles, a reduced RH in the cloudy layer (different curves in each panel in Fig. 2) would enhance the entrainment (by mixing drier environmental air into the cloud) and therefore, N_{op} would decrease. However, for profiles with a similar RH in the cloudy layer, a reduction in the inversion base height would change the cloud's size and the cloud's surface-area-to-volume ratio. This again changes the portion of the cloud that is influenced by the drier ambient air and strengthens the entrainment. Smaller clouds have a higher surface-area-to-volume ratio and therefore the entrainment plays a more important role. This is reflected by the smaller N_{op} values for the smaller clouds.

The ratio of the cloud's surface area to volume (η) can serve as a measure of the balance between core and margin-based processes in clouds. The internal (cloud-core based) processes are more adiabatic in nature (since the core is less exposed to entrainment) (Wang et al., 2009) and therefore, for given temperature and humidity profiles, they are less affected by the suppressing branch of the aerosol effect. Therefore, higher aerosol loading yields more efficient condensation (a larger droplet surface area) for a longer time (owing to the postponement in the collision-coalescence process). On the other hand, over the cloud's periphery, more aerosols enhance the evaporation and the mixing with the outer air.

This impact of aerosol loading on the magnitude and timing of the core vs. the periphery-based cloud's processes is reflected in the response of different cloud features. Figure 6 presents 3 clouds' properties for each simulation as a function of the aerosol concentration (each curve represents 10 simulations of specific profiles): (1) the maximum cloud top height per simulation (defined by the height level of 0.01 g kg^{-1} liquid water content, top panels), (2) the maximum (over the cloud's lifetime) of the mean cloud's updraft (middle panels). This measure is calculated as the mean updraft of all the cloud grid points, weighted by the liquid water mass of each grid point, and (3) the total amount of surface rain (bottom panels). A similar reversal trend with a clear extreme was observed for all 9 profiles for all 3 measures. For the three cloud features

ACPD
14, 23555–23581, 2014

shown, the optimal concentration per atmospheric profile is at a slightly higher aerosol loading compared with the N_{op} value, which was defined as the optimum aerosol concentration for the maximum in the total mass. The peak in the values of the cloud features that are controlled by the cloud's core processes (less affected by entrainment) corresponds to larger aerosol loading values compared with features that are more sensitive to margin-based processes. Eventually, since all the processes are coupled, the enhancement in the margins' effects results in a weakening of the core-based processes as well. The maximum total mass of the cloud is more sensitive to the cloud margins' processes than the cloud's maximum top height (which is located above the cloud's core).

Similarly, since the mean updraft weighted by the liquid water mass is less sensitive to aerosol effects on the lighter margins, the declining branch is less significant.

Rain is in many ways the end result of all the cloud processes; the total condensed and evaporated mass controls the cloud's total water mass together with the collision-coalescence process that drives the formation of the rain drops.

An optimal aerosol concentration, followed by a reverse in the sign of the trend, is also shown for the rain (as can be seen in Fig. 6, bottom panel). The aerosol concentration value that corresponds to the maximal rain yield (per initialization profile) usually increases for profiles with a higher inversion base height and/or a more humid environment in the cloudy layer, and in most cases these values are higher than N_{op} (in 8 out of the 9 initial profiles). As a first approximation, rain is expected to scale well with the total water mass (neglecting the evaporation of rain below the cloud), this suggests similarities in the optimal aerosol concentration for total mass and rain. So why does the maximum in the surface rain yields correspond to larger optimal aerosol concentrations?

The reason is the dependency of rain on the collection efficiency. The collection efficiency increases with both the number concentration and the variance of the droplet size distribution. Thus aerosols would have a contradictory effect on the collection efficiency. At low values of aerosol concentrations, as the aerosol loading increases, a few

ACPD
14, 23555–23581, 2014

big lucky drops (Kostinski and Shaw, 2005) that initiate the rain can collect more small drops and consequently produce more rain yield. This trend continues until the effect of the smaller variance of the droplet size distribution (with increasing aerosol loading) becomes more important. The aerosol concentration that corresponds to the maximum collection efficiency for a given profile is slightly higher then N_{op}.

Finally it should be noted that those cases involving small warm clouds (profile T3) show less sensitivity to the RH and as expected, have low values of optimal aerosol concentrations. N_{op} values were shown to be $\sim 25\,cm^{-3}$ for the T3 cases (Fig. 2), suggesting that under our current atmospheric conditions, apart from the extremely pristine places, the local aerosol concentrations are larger than the optimal value, locating the clouds already on the descending branch. Similarly, the clouds' top height, for the T3 cases, shows relatively low sensitivity to aerosol loading, with optimal concentrations of $\sim 100\,cm^{-3}$ (Fig. 6).

These rather basic results may bridge the ongoing gap between observations and the modeling of aerosol effects on warm convective clouds. Many of the numerical studies of warm convective clouds focus on trade-like cumulus clouds (Jiang et al., 2006, 2009, 2010; Xue and Feingold, 2006; Xue et al., 2008; Koren et al., 2009; Seigel, 2014) where the characteristic cloud size is around 1 km. However, earth-observing satellite instruments (such as MODIS) are biased toward much larger clouds (Kaufman et al., 2005; Yuan et al., 2011; Koren et al., 2014). Therefore, our results suggest that warm clouds simulations will "see" the descending branch of the trend, whereas satellites will be biased toward larger clouds that can "enjoy" higher aerosol levels before reaching the optimum.

4 Summary

Cloud properties are controlled by both the thermodynamic conditions and by the aerosol properties. Here we aimed at studying the interplay between these main players for warm clouds. Although using a single cloud model that cannot capture pro-

ACPD
14, 23555–23581, 2014

cesses in a cloud-field scale, we found a very rich interplay between key warm processes that shed new light on previous results found by numerical models and observations. More specifically, we showed that a reversal in the trend sign takes place when initially a cloud mass increases with aerosol loading up to a turning point, defined here as the optimal concentration, N_{op}, followed by a decrease in the maximal cloud mass. This reversal in trend sign was shown to be applicable to other cloud properties such as the cloud's top height, updraft, and rain; however, the optimal concentration is not the same as the one for the total mass. The dependency of N_{op} on the thermodynamic conditions was examined. Specifically, we showed that more unstable temperature profiles and higher relative humidity enable larger N_{op} values, namely, clouds are aerosol-limited up to higher aerosol concentrations.

The existence of an optimal concentration results from two competing effects. On the one hand, more aerosols provide a larger droplet surface area for condensation and delay the onset of collection processes, and therefore drive stronger latent heat release and more condensed mass to be formed and to be pushed upward. On the other hand, more aerosols result in stronger entrainment and a stronger drag force (driven by the larger mass) that suppress the cloud's development. In that respect, we noted that invigoration effects are more associated with cloud core-based processes where the cloud is closer to adiabatic and the likelihood of larger supersaturation is higher. On the other hand, cloud suppression effects are likely to occur more in the cloud's peripheral regions where unsaturated, drier air enters the cloud.

Such opposite associations with respect to the location within the cloud imply that the total cloud surface-area-to-volume ratio (defined here as η) is an informative parameter. For larger η values, a stronger effect of the periphery-oriented processes is expected to influence the cloud's fate. Therefore, for profiles that support only small convective cloud formations (lower inversion and lower environmental RH), η would have larger values and therefore smaller N_{op} concentrations. This suggests that for most cases in nature (where the atmospheric conditions are between slightly and strongly polluted) small clouds would be beyond their N_{op} values, on the descending branch of the trend

ACPD
14, 23555–23581, 2014

(suppression effect). On the other hand, profiles that support deeper convection (high inversion and high environmental RH) would produce deeper clouds with smaller η values and therefore larger N_{op} concentrations. This can be translated to a higher likelihood of finding in nature deeper clouds that are aerosol limited and consequently, on the ascending (invigoration) branch. Such a view bridges the gap between conflicting reports from numerical model studies that tend to simulate small trade-like clouds and mostly report on suppression by aerosols and observations that, owing to pixel resolution, are biased toward larger clouds and mostly report on invigoration.

In this paper we discuss the importance of both the timing and the magnitude of processes, but in order to reduce the complexity, we discussed the time evolution of the clouds only briefly. We compared the onset or maximal values of processes instead of the entire evolution. Such a view captures well and in a condensed way the overall results but not the whole story. For example, it is obvious that the increase in condensation efficiency by aerosols will reach a saturation stage, in which the characteristic time for consuming the available water vapors is much smaller compared with the advection timescale (Pinsky et al., 2013). We could see this in our results when we compared the condensation curves of the 1000 and 4000 cm^{-3} cases (Fig. 3). The condensation curve is similar and most of the effect is driven by the delay in the collection processes. In many ways the core vs. the periphery-based processes view can be linked to the time evolution of a cloud. The early stages of the cloud are more adiabatic, whereas the dissipation stage of the cloud, by definition, is controlled more by periphery-based processes. Therefore, we can conclude that even during a single cloud evolution more aerosols can be translated to invigoration in the early stages and to suppression in the later ones. The question addressed in this paper is what factor dominates and what the overall result is.

Similarly, throughout the paper we discuss drag forces as a factor that opposes invigoration. This again is accurate from the end-results viewpoint. When it is examined from the time perspective of one given cloud, enhanced drag forces can be viewed not only as opposing, but also as a result of invigoration, i.e. “enjoy now and pay later”. Drag

ACPD
14, 23555–23581, 2014

forces are scaled with mass; therefore, an invigorated cloud that "enjoys" the benefits of more aerosols during the early stages (when the profile is unstable enough and the RH is high and therefore N_{op} is large) will "pay" at later stages when it carries a large accumulated mass that enhances the drag force. Thus, again the timing perspective is extremely important and provides a much richer view of the problem.

Acknowledgements. The research leading to these results received funding from the European Research Council (ERC) under the European Union's Seventh Framework Programme (FP7/2007-2013)/ERC Grant agreement no. 306965 (CAPRI).

References

Albrecht, B. A.: Aerosols, cloud microphysics, and fractional cloudiness, Science, 245, 1227–1230, doi:10.1126/science.245.4923.1227, 1989.

Altaratz, O., Koren, I., and Reisin, T.: Humidity impact on the aerosol effect in warm cumulus clouds, Geophys. Res. Lett., 35, L17804, doi:10.1029/2008GL034178, 2008.

Altaratz, O., Koren, I., Remer, L., and Hirsch, E.: Review: cloud invigoration by aerosols – coupling between microphysics and dynamics, Atmos. Res., 140, 38–60, 2014.

Andreae, M. O., Rosenfeld, D., Artaxo, P., Costa, A. A., Frank, G. P., Longo, K. M., and Silva-Dias, M. A. F.: Smoking rain clouds over the Amazon, Science, 303, 1337–1342, doi:10.1126/science.1092779, 2004.

Baker, M. B. and Peter, T.: Small-scale cloud processes and climate, Nature, 451, 299–300, doi:10.1038/nature06594, 2008.

Boucher, O., Randall, D., Artaxo, P., Bretherton, C., Feingold, G., Forster, P., Kerminen, V.-M., Kondo, Y., Liao, H., Lohmann, U., Rasch, P., Satheesh, S. K., Sherwood, S., Stevens, B., and Zhang, X. Y.: Clouds and Aerosols. In: Climate Change 2013: The Physical Science Basis. Contribution of Working Group I to the Fifth Assessment Report of the Intergovernmental Panel on Climate Change, edited by: Stocker, T. F., Qin, D., Plattner, G.-K., Tignor, M., Allen, S. K., Boschung, J., Nauels, A., Xia, Y., Bex, V., and Midgley, P. M., Cambridge University Press, Cambridge, United Kingdom and New York, NY, USA, 2013.

ACPD
14, 23555–23581, 2014

Fan, J., Leung, L. R., Rosenfeld, D., Chen, Q., Li, Z., Zhang, J., and Yan, H.: Microphysical effects determine macrophysical response for aerosol impacts on deep convective clouds, P. Natl. Acad. Sci. USA, 110, E4581–E4590, 2013.

Feingold, G., Cotton, W. R., Kreidenweis, S. M., and Davis, J. T.: The impact of giant cloud condensation nuclei on drizzle formation in stratocumulus: implications for cloud radiative properties, J. Atmos. Sci., 56, 4100–4117, doi:10.1175/1520-0469(1999)056<4100:tiogcc>2.0.CO;2, 1999.

Fitzgerald, J. and Spyers-Duran, P.: Changes in cloud nucleus concentration and cloud droplet size distribution associated with pollution from St. Louis, J. Appl. Meteorol., 12, 511–516, 1973.

Forster, P., Ramaswamy, V., Artaxo, P., Berntsen, T., Betts, R., Fahey, D. W., Haywood, J., Lean, J., Lowe, D. C., Myhre, G., Nganga, J., Prinn, R., Raga, G., Schulz, M., and Van Dorland, R.: Changes in Atmospheric Constituents and in Radiative Forcing, in: Climate Change 2007: The Physical Science Basis. Contribution of Working Group I to the Fourth Assessment Report of the Intergovernmental Panel on Climate Change, edited by: Solomon, S., Qin, D., Manning, M., Chen, Z., Marquis, M., Averyt, K. B., Tignor, M., and Miller, H. L., Cambridge University Press, Cambridge, United Kingdom and New York, NY, USA, 2007.

Gunn, R. and Phillips, B.: An experimental investigation of the effect of air pollution on the initiation of rain, J. Meteorol., 14, 272–280, 1957.

Jaenicke, R.: Aerosol physics and chemistry, Landolt-Bornstein Neue Serie 4b, edited by: Fischer, G., Springer-Verlag Berlin, 391–457, 1988.

Jiang, H., Xue, H., Teller, A., Feingold, G., and Levin, Z.: Aerosol effects on the lifetime of shallow cumulus, Geophys. Res. Lett., 33, L14806, doi:10.1029/2006GL026024, 2006.

Jiang, H., Feingold, G., and Koren, I.: Effect of aerosol on trade cumulus cloud morphology, J. Geophys. Res.-Atmos., 114, D11209, doi:10.1029/2009JD011750, 2009.

Jiang, H., Feingold, G., and Sorooshian, A.: Effect of aerosol on the susceptibility and efficiency of precipitation in warm trade cumulus clouds, J. Atmos. Sci., 67, 3525–3540, 2010.

Jiang, H. L. and Feingold, G.: Effect of aerosol on warm convective clouds: aerosol-cloud-surface flux feedbacks in a new coupled large eddy model, J. Geophys. Res.-Atmos., 111, D01202, doi:10.1029/2005jd006138, 2006.

Kaufman, Y. J., Koren, I., Remer, L. A., Rosenfeld, D., and Rudich, Y.: The effect of smoke, dust, and pollution aerosol on shallow cloud development over the Atlantic Ocean, P. Natl. Acad. Sci. USA, 102, 11207–11212, doi:10.1073/pnas.0505191102, 2005.

ACPD
14, 23555–23581, 2014

Khain, A. P.: Notes on state-of-the-art investigations of aerosol effects on precipitation: a critical review, Environ. Res. Lett., 4, 015004, doi:10.1088/1748-9326/4/1/015004, 2009.
Koren, I., Kaufman, Y. J., Rosenfeld, D., Remer, L. A., and Rudich, Y.: Aerosol invigoration and restructuring of Atlantic convective clouds, Geophys. Res. Lett., 32, L14828, doi:10.1029/2005GL023187, 2005.
Koren, I., Feingold, G., Jiang, H., and Altaratz, O.: Aerosol effects on the inter-cloud region of a small cumulus cloud field, Geophys. Res. Lett., 36, L14805, doi:10.1029/2009GL037424, 2009.
Koren, I., Altaratz, O., Remer, L. A., Feingold, G., Martins, J. V., and Heiblum, R. H.: Aerosol-induced intensification of rain from the tropics to the mid-latitudes, Nat. Geosci., 118–122, doi:10.1038/NGEO1364, 2012.
Koren, I., Dagan, G., and Altaratz, O.: From aerosol-limited to invigoration of warm convective clouds, Science, 344, 1143–1146, 2014.
Kostinski, A. B. and Shaw, R. A.: Fluctuations and luck in droplet growth by coalescence, B. Am. Meteorol. Soc., 86, 235–244, 2005.
Levin, Z. and Cotton, W. R. (Eds.): Aerosol Pollution Impact on Precipitation: a Scientific Review, Springer Press, the Netherlands, 382 pp., 2009.
Li, Z., Niu, F., Fan, J., Liu, Y., Rosenfeld, D., and Ding, Y.: Long-term impacts of aerosols on the vertical development of clouds and precipitation, Nat. Geosci., 4, 888–894, doi:10.1038/ngeo1313, 2011.
Pinsky, M., Mazin, I., Korolev, A., and Khain, A.: Supersaturation and diffusional droplet growth in liquid clouds, J. Atmos. Sci., 70, 2778–2793, 2013.
Pruppacher, H. R. and Klett, J. D.: Microphysics of clouds and precipitation, D. Reidel Publishing company, Dordrecht, the Netherlands, 706 pp., 1978.
Reisin, T., Levin, Z., and Tzivion, S.: Rain production in convective clouds as simulated in an axisymmetric model with detailed microphysics. Part I: Description of the model, J. Atmos. Sci., 53, 497–519, doi:10.1175/1520-0469(1996)053<0497:RPICCA>2.0.CO;2, 1996.
Reutter, P., Su, H., Trentmann, J., Simmel, M., Rose, D., Gunthe, S. S., Wernli, H., Andreae, M. O., and Pöschl, U.: Aerosol- and updraft-limited regimes of cloud droplet formation: influence of particle number, size and hygroscopicity on the activation of cloud condensation nuclei (CCN), Atmos. Chem. Phys., 9, 7067–7080, doi:10.5194/acp-9-7067-2009, 2009.

ACPD
14, 23555–23581, 2014

Rosenfeld, D., Lohmann, U., Raga, G. B., O'Dowd, C. D., Kulmala, M., Fuzzi, S., Reissell, A., and Andreae, M. O.: Flood or drought: how do aerosols affect precipitation?, Science, 321, 1309–1313, doi:10.1126/science.1160606, 2008.
Seigel, R. B.: Shallow Cumulus Mixing and Subcloud Layer Responses to Variations in Aerosol Loading, J. Atmos. Sci., 71, 2581–2603, doi:10.1175/JAS-D-13-0352.1, 1978.
Simpson, J.: On cumulus entrainment and one-dimensional models, J. Atmos. Sci., 28, 449–455, 1971.
Small, J. D., Chuang, P. Y., Feingold, G., and Jiang, H.: Can aerosol decrease cloud lifetime?, Geophys. Res. Lett., 36, L16806, doi:10.1029/2009GL038888, 2009.
Squires, P.: The microstructure and colloidal stability of warm clouds, Tellus, 10, 262–271, 1958.
Squires, P. and Twomey, S.: The relation between cloud droplet spectra and the spectrum of cloud nuclei, Geoph. Monog. Series, 5, 211–219, 1960.
Stirling, A. and Stratton, R.: Entrainment processes in the diurnal cycle of deep convection over land, Q. J. Roy. Meteor. Soc., 138, 1135–1149, 2012.
Tao, W.-K., Chen, J.-P., Li, Z., Wang, C., and Zhang, C.: Impact of aerosols on convective clouds and precipitation, Rev. Geophys., 50, RG2001, doi:10.1029/2011RG000369 2012.
Twomey, S.: The influence of pollution on the shortwave albedo of clouds, J. Atmos. Sci., 34, 1149–1152, 1977.
Tzivion, S., Feingold, G., and Levin, Z.: An efficient numerical solution to the stochastic collection equation, J. Atmos. Sci., 44, 3139–3149, 1987.
Tzivion, S., Reisin, T., and Levin, Z.: Numerical simulation of hygroscopic seeding in a convective cloud, J. Appl. Meteorol., 33, 252–267, 1994.
Wang, Y., Geerts, B., and French, J.: Dynamics of the cumulus cloud margin: an observational study, J. Atmos. Sci., 66, 3660–3677, 2009.
Warner, J.: A reduction in rainfall associated with smoke from sugar-cane fires-An inadvertent weather modification?, J. Appl. Meteorol., 7, 247–251, 1968.
Warner, J. and Twomey, S.: The production of cloud nuclei by cane fires and the effect on cloud droplet concentration, J. Atmos. Sci., 24, 704–706, 1967.
Wilson, C. T. R.: Condensation of water vapour in the presence of dust-free air and other gases, P. R. Soc. London, 61, 240–242, 1897.
Xue, H. and Feingold, G.: Large-eddy simulations of trade wind cumuli: investigation of aerosol indirect effects, J. Atmos. Sci., 63, 1605–1622, 2006.

ACPD
14, 23555–23581, 2014

Xue, H., Feingold, G., and Stevens, B.: Aerosol effects on clouds, precipitation, and the organization of shallow cumulus convection, J. Atmos. Sci., 65, 392–406, doi:10.1175/2007jas2428.1, 2008.

Yin, Y., Levin, Z., Reisin, T. G., and Tzivion, S.: The effects of giant cloud condensation nuclei on the development of precipitation in convective clouds – a numerical study, Atmos. Res., 53, 91–116, 2000.

Yuan, T., Remer, L. A., and Yu, H.: Microphysical, macrophysical and radiative signatures of volcanic aerosols in trade wind cumulus observed by the A-Train, Atmos. Chem. Phys., 11, 7119–7132, doi:10.5194/acp-11-7119-2011, 2011.

ACPD

14, 23555–23581, 2014

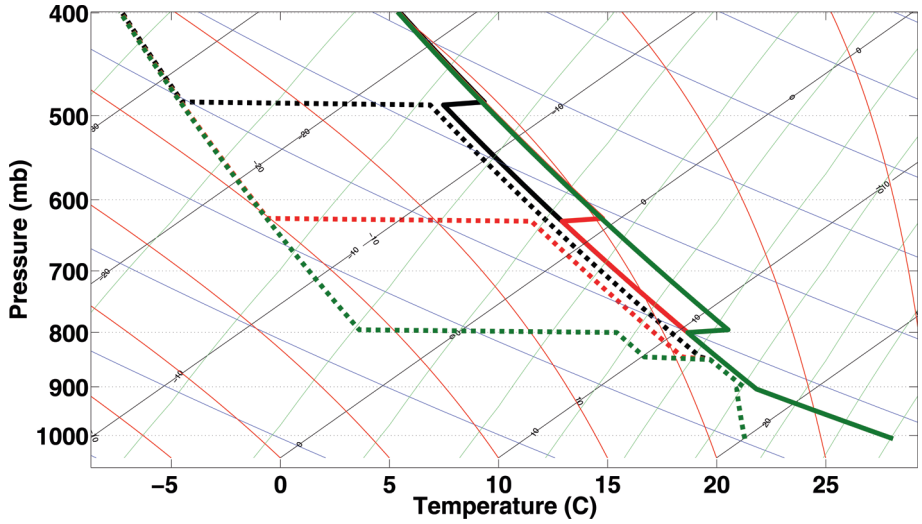

Figure 1. Thermodynamic diagram presenting examples of 3 of the initial atmospheric profiles T1RH1 (black), T2RH2 (red), and T3RH3 (green). Solid lines denote temperature profiles and dashed lines dew-point temperature. In total we run simulations for 9 different initialization profiles.

ACPD
14, 23555–23581, 2014

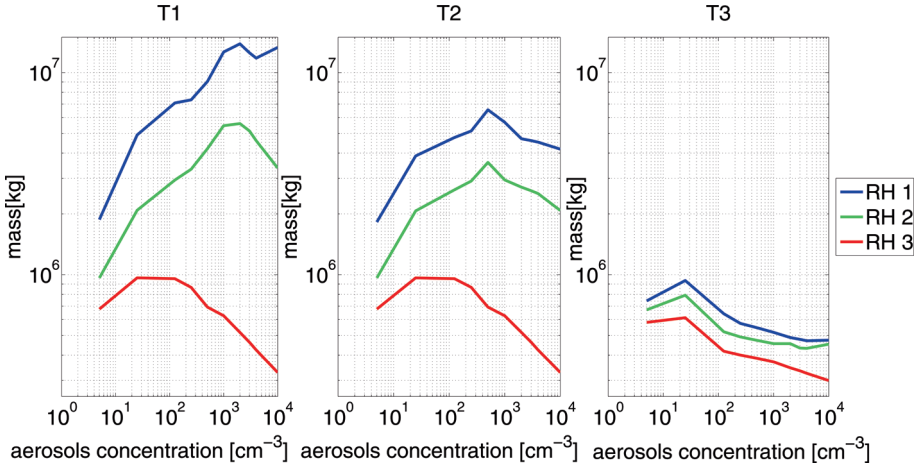

Figure 2. The maximum cloud total mass for each simulated cloud as a function of the aerosol concentration used in the simulation. Each curve represents 10 simulations conducted using the same atmospheric profile (a total of 9 different initialization profiles). T1 represents a profile with an inversion layer located at 6 km, T2 at 4 km, and T3 at 2 km. RH1 represents a profile with 95 % RH in the cloudy layer, RH2-90 %, and RH3-80 %.

ACPD
14, 23555–23581, 2014

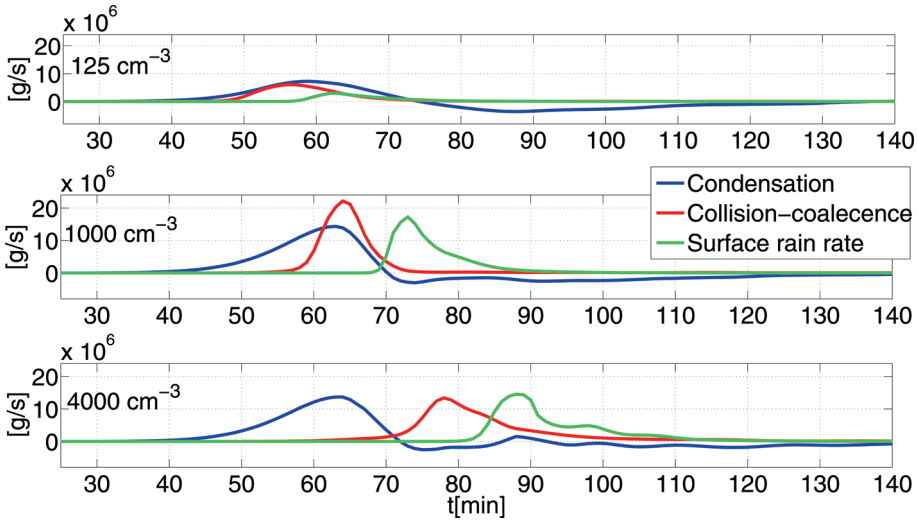

Figure 3. The total condensed/evaporated mass per unit time (blue), the total collected mass per unit time (red) and the surface rain mass (green) as a function of time for three clouds with aerosol levels of 125 (upper panel), 1000 (middle panel), and 4000 cm^{-3} (lower panel) of profile T1RH1.

ACPD
14, 23555–23581, 2014

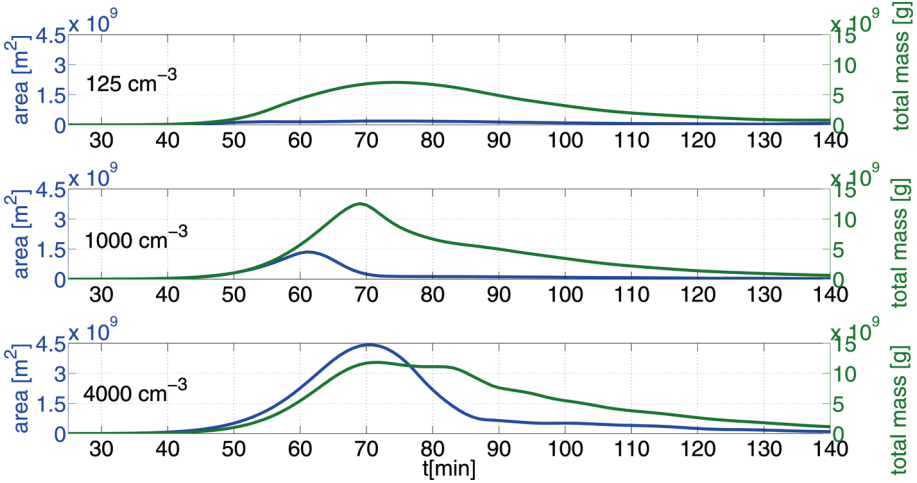

Figure 4. The total cloud water mass (green) and the total droplet surface area (blue) as a function of time for three clouds with aerosol levels of 125 (upper panel), 1000 (middle panel), and 4000 cm^{-3} (lower panel) for profile T1RH1.

ACPD
14, 23555–23581, 2014

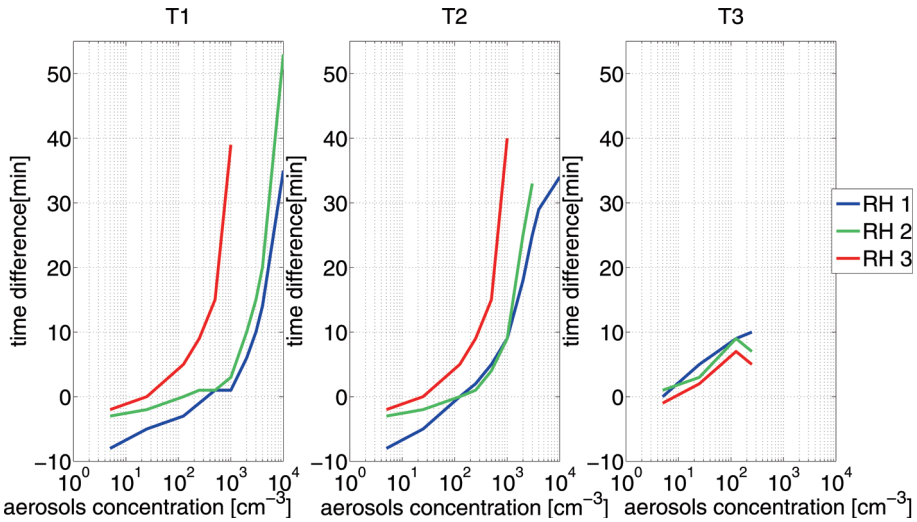

Figure 5. The time difference between the maximum collected mass per unit time and the maximum condensed mass per unit time for each simulated cloud as a function of the aerosol concentration. T1 represents a profile with an inversion layer located at 6 km, T2 at 4 km, and T3 at 2 km. RH1 represents a profile with 95 % RH in the cloudy layer, RH2-90 %, and RH3-80 %. Each curve represents 10 simulations performed for an initialization profile (a total of 9 profiles).

ACPD
14, 23555–23581, 2014

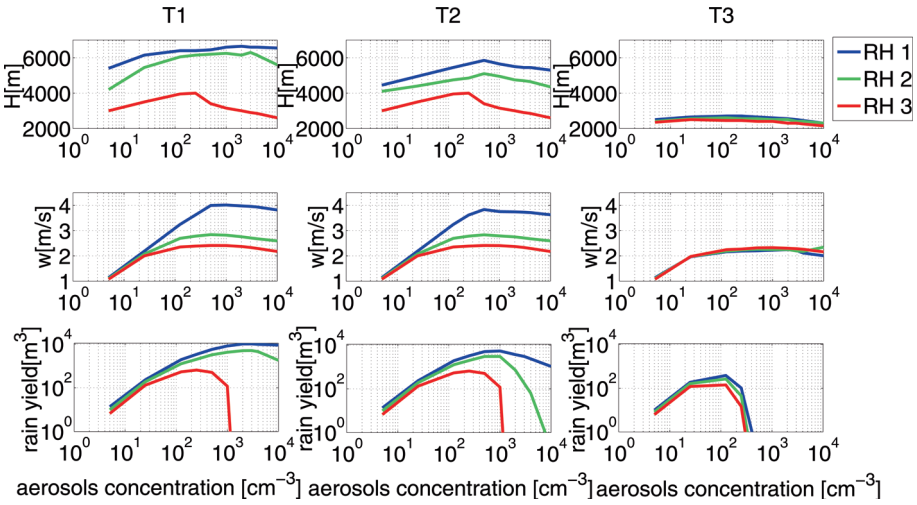

Figure 6. The cloud's maximum top height (top panels), the maximum over time of the mean vertical velocity weighted by the mass in each grid point (middle panels) and the total surface rain yield (bottom panels) as a function of the aerosol loading, for each simulated cloud as a function of the aerosol concentration. Each curve represents 10 simulations performed for an initialization profile (a total of 9 profiles).

ACPD
14, 23555–23581, 2014